J Math Chem (2009) 45:161–174
DOI 10.1007/s10910-008-9374-7

ORIGINAL PAPER

Calculating the surface tension between a flat solid and a liquid: a theoretical and computer simulation study of three topologically different methods

Uriel Octavio Moreles Vázquez · Wataru Shinoda · Preston B. Moore · Chi-cheng Chiu · Steven O. Nielsen

Received: 10 August 2007 / Accepted: 15 November 2007 / Published online: 18 June 2008

Abstract We discuss three topologically different methods for calculating the surface tension between a flat solid and a liquid from theoretical and computer simulation viewpoints. The first method, commonly used in experiments, measures the contact angle at which a static droplet of liquid rests on a solid surface. We present a new analysis algorithm for this method and explore the effects of line tension on the contact angle. The second method, commonly used computer simulations, uses the pressure tensor through the virial in a system where a thick, infinitely extended slab of liquid rests on a solid surface. The third method, which is original to this paper and is closest to the thermodynamic definition of surface tension, applies to a spherical solid in contact with liquid in which the flat solid is recovered by extrapolating the sphere radius to infinity. We find that the second and third methods agree with each other, while the first method systematically underestimates surface tension values.

Keywords Surface tension · Solvation free energy · Solid/liquid interface · Contact angle · Line tension

U. O. M. Vázquez
Universidad de Guanajuato, Facultad de Matemáticas, A.P. 402, Guanajuato 36240 Gto., Mexico

W. Shinoda
Research Institute for Computational Sciences, National Institute of Advanced Industrial Science and Technology (AIST), Central 2, 1-1-1, Umezono, Tsukuba, Ibaraki 305-8568, Japan

P. B. Moore
Department of Chemistry & Biochemistry, University of the Sciences in Philadelphia, Philadelphia, PA 19104, USA

C.-c. Chiu · S. O. Nielsen (✉)
Department of Chemistry, The University of Texas at Dallas, 2601 North Floyd Road, Richardson, TX 75080, USA
e-mail: steven.nielsen@utdallas.edu
URL: http://www.utdallas.edu/∼son051000

1 Introduction

The surface tension, γ, between a liquid and a solid is a fundamental ingredient in the behavior and control of a wide range of systems. For example, nanoparticles can be directed to self-assemble into thin films at an oil/water interface by manipulating the solid/water and solid/oil surface tensions [1]. Since these assemblies stabilize water-in-oil or oil-in-water droplets, they hold great promise for encapsulation and tunable delivery strategies [2].

Although the solid/liquid surface tensions are thought to be the most fundamental ingredient in controlling these systems, it is not possible to directly measure water/nanoparticle and oil/nanoparticle surface tensions by experiment. This is discussed by Binks and Clint [3], who estimate the surface tensions on theoretical grounds. However, such estimates are approximate due to the many assumptions used. In contrast, computer simulations offer the possibility of accurately computing such surface tensions. This article uses three methods to compute the solid/liquid surface tension for flat solids. The focus is on implementation in molecular dynamics (MD) computer simulations. The third method also allows the calculation of the surface tension between a solid spherical nanoparticle and a liquid, which makes a direct link to the motivating example given above. In what follows we present the three methods and discuss the relationships between them. Along these same lines, we would like to bring to the reader's attention the elegant paper by Salomons [4].

2 Method 1: contact angle

The contact angle of a static droplet of liquid on a flat solid surface represents a state of mechanical equilibrium, and as such is determined by a balance between three interfacial tensions: the liquid/vapor surface tension, γ_{lv}, the solid/vapor surface tension, γ_{sv}, and the solid/liquid interfacial tension, γ_{sl} (see Fig. 1). Each pair of phases meets on a two-manifold called an interface, and all three phases meet on a one-manifold called the three-phase line. For each point on the three-phase line there are three vectors, one for each interface, that act perpendicularly to the three-phase line and tangentially to their corresponding interface. The equilibrium relation between these vectors is known as Young's equation, where θ is the Young contact angle.[1]

$$\gamma_{\mathrm{lv}} \cos\theta = \gamma_{\mathrm{sl}} - \gamma_{\mathrm{sv}}. \tag{1}$$

However, Young's equation is only valid for macroscopic droplets. For microscopic droplets, the contact angle is influenced by the three-phase solid/liquid/vapor contact line, which contributes an additional energy per unit length called the line tension τ [5]. The modified Young's equation accounts for the effect of line tension, where R is the radius of the base of the droplet (in contact with the solid).

[1] Note that some authors define the Young contact angle as $(\pi - \theta)$, which changes the Young equation in a trivial manner.

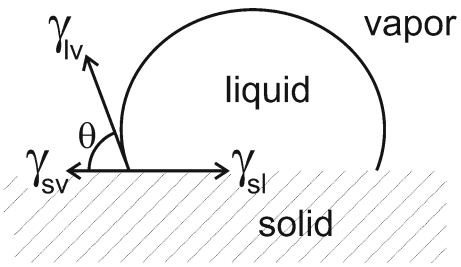

Fig. 1 Mechanical equilibrium, expressed through the three two-phase interfacial tension values, determines the contact angle θ at which a static liquid droplet rests on a flat solid surface. By definition, the surface is classified as hydrophobic if the contact angle for a droplet of water is acute (as shown). An obtuse angle corresponds to a hydrophilic surface

$$\gamma_{\mathrm{lv}} \cos\theta = \gamma_{\mathrm{sl}} - \gamma_{\mathrm{sv}} + \frac{\tau}{R}. \tag{2}$$

By considering the contact angle as a function of the droplet base radius, $\theta = \theta(R)$ and using two different radii R, R', we obtain

$$\gamma_{\mathrm{sl}} - \gamma_{\mathrm{lv}} \cos\theta(R) + \frac{\tau}{R} = \gamma_{\mathrm{sv}} = \gamma_{\mathrm{sl}} - \gamma_{\mathrm{lv}} \cos\theta(R') + \frac{\tau}{R'} \tag{3}$$

or

$$\cos\theta(R) = \cos\theta(R') + \frac{\tau}{\gamma_{\mathrm{lv}}}\left(\frac{1}{R} - \frac{1}{R'}\right) \longrightarrow \cos\theta_\infty + \frac{\tau}{\gamma_{\mathrm{lv}} R} \quad \text{as} \quad R' \to \infty, \tag{4}$$

where θ_∞ is the limit of $\theta(R')$ as $R' \to \infty$, provided this limit exists. We can thus write

$$\cos\theta(R) = f\left(\frac{1}{R}\right) = \cos\theta_\infty + \frac{\tau}{\gamma_{\mathrm{lv}}}\left(\frac{1}{R}\right), \tag{5}$$

where the function $f(1/R)$ is a straight line with slope $\tau/\gamma_{\mathrm{lv}}$ and intercept $\cos\theta_\infty$.

From three equilibrium MD simulations of a droplet composed of different numbers of atoms, N_1, N_2, N_3, it is possible to find $\cos\theta_\infty$ by measuring the radii and angles R_i, θ_i, plotting the points $(1/R_i, \cos\theta_i)$ for $i = 1, 2, 3$ and extrapolating to an infinite radius with a straight line.

To determine the contact angle $\theta(R)$, two steps are required. The liquid/vapor boundary must be identified and the contact angle must be measured from this boundary. Two different approaches are taken in the literature once the boundary has been identified. Werder [6] employs a circular best fit to estimate the contact angle. In contrast, Giovambattista [7] makes no geometrical assumptions about the drop profile, and fits the boundary data with the function $f(z) = Az^2 + Bz + C$ where z is the distance of a water molecule from the surface. Our simulation data suggests that no geometrical assumption about the boundary points should be made, other than they be convex. Our approach makes use of a particular class of spline functions, described below.

For the liquid, we use the recent coarse grain water model of Shinoda [8]. The potential energy between water sites is given by $u_{ll}(r) = 3\sqrt{3}\epsilon/2[(\sigma/r)^{12}$

$-(\sigma/r)^4]$, where r is the distance between the sites, and where $\epsilon = 0.895$ kcal/mol, $\sigma = 0.437$ nm. We choose $N_1 = 11,000$, $N_2 = 22,000$, and $N_3 = 44,000$ for the number of water sites in a liquid droplet. The potential energy between an infinitely extended flat solid and a liquid particle is given by [9] $U_{\rm sl}(d) = a\epsilon\sigma^9 d^{-6} - b\epsilon\sigma^6 d^{-3}$, with $a = 0.0338$, $b = 0.118$, and $\sigma = 0.4$ nm. The value of ϵ determines whether, and to what extent, the solid object is hydrophobic or hydrophilic. d is the distance between the liquid particle and the solid. The droplet base radius R_i and contact angle $\theta_i = \theta(R_i)$ are measured from a room temperature MD simulation as follows: after the droplet has equilibrated from an initial hemispherical geometry where the solid occupies the region $z \leq 0$ (1 ns), the spatial coordinates of all the liquid atoms are saved every 40 ps. To determine R_i, we choose a small $\epsilon > 0$ and project the liquid particles in the region $0 < z < \epsilon$ onto the plane $z = 0$ for each set of coordinates, giving a diffuse circle. We then identify the boundary of this circle, which is the three-phase contact line, by applying the following algorithm: every point on the boundary has the special property that there is a line passing through it which divides the plane $z = 0$ into two regions: a region containing all the other points, and an empty region. We note that this boundary algorithm is valid for convex sets only, and that in practice one must allow a few points in the "empty" region due to thermal fluctuations.

For a circle of radius R centered at the origin, the distance to a point (x_j, y_j) on the circular boundary identified above is $|(x_j^2 + y_j^2)^{1/2} - R|$. In order to find the radius which best fits these points, we need to minimize the function $f(R) = \sum_{j=1}^{N}((x_j^2 + y_j^2)^{1/2} - R)^2$ where N is the number of points on the boundary. The minimum is $R = \sum_{j=1}^{N}(x_j^2 + y_j^2)^{1/2}/N$ which is simply the average of the distances of the boundary points from the center. Figure 2 gives an idea of the procedure. A final average is taken over the sets of coordinates sampled at different times from the equilibrium simulation to give R_i.

To determine the contact angle $\theta(R_i)$ we average over thin slices of the droplet normal to the solid/liquid interface and passing through the center of the droplet (identified as the center of the three-phase circular boundary), as well as over sets of

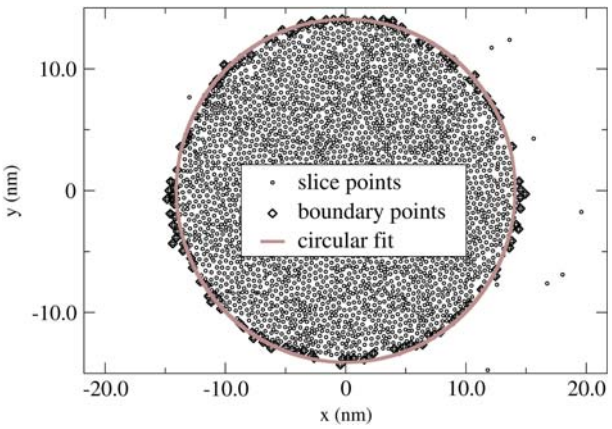

Fig. 2 A parallel slice, closest to the surface, of a liquid droplet resting on a flat solid surface is shown for a hydrophilic surface with $\epsilon = 270$. The solid/liquid/vapor three-phase boundary points are identified and fit to a circle to measure the three-phase radius

droplet coordinates spaced 40 ps apart from each other in time. The coordinates of the liquid particles in each slice are projected onto the plane normal to the solid/liquid interface and passing through the droplet center. An analogous algorithm is used to identify the boundary of the projected slice, which is the liquid/vapor interface. A smooth curve is drawn through the boundary points using a cubic spline function based on the algorithm proposed by Reinsch [10].

The spline function is two times differentiable, built piecewise over intervals $[x_i, x_{i+1}]$ from cubic polynomials. Since we do not use parametric splines, we divide the droplet into two halves using a dividing line normal to the solid/liquid interface, rotate the droplet by $\pi/2$, apply the spline separately to the two halves, and then rotate back by $-\pi/2$. We do not attempt to fit the spline to the droplet coordinates farthest from the solid surface. Figure 3 gives an idea of this procedure. The spline minimizes

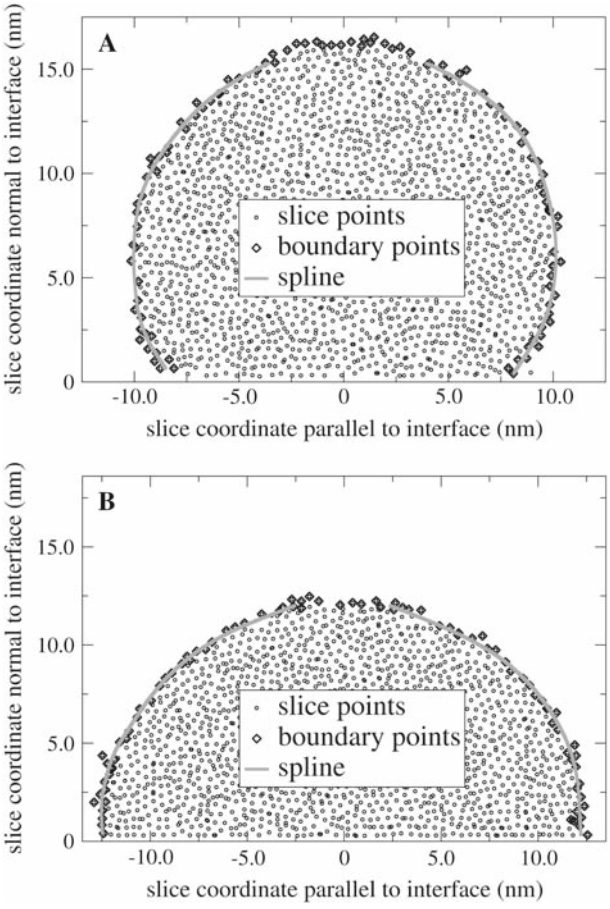

Fig. 3 Shown are perpendicular slices of a liquid droplet resting on a flat solid surface. Panel A corresponds to a hydrophobic surface ($\theta < \pi/2$) with $\epsilon = 110$, while panel B corresponds to a neutral surface ($\theta \approx \pi/2$) with $\epsilon = 230$. The liquid/vapor boundary points are identified and fit to a spline function as explained in the text. The contact angle is then calculated from the spline polynomial closest to the solid surface

$$\int_{x_0}^{x_n} g''(x)^2 \, \mathrm{d}x \tag{6}$$

among all functions $g(x)$ such that

$$\sum_{i=0}^{n} \left(\frac{g(x_i) - y_i}{\delta y_i} \right)^2 \leq S, \quad g \in C^2[x_0, x_n], \tag{7}$$

where δy_i and S are parameters that control the smoothness of the curve. We take $S = N - (2N)^{1/2}$ where N is the number of points that the spline is approximating (the number of boundary points in the left or right hand side of one slice). This is consistent with the value range recommended by Reinsch [10], namely $N-(2N)^{1/2} \leq S \leq N + (2N)^{1/2}$.

The parameter δy is fixed for each boundary spline, but varies over slice angles and time. Specifically, δy is initially taken as 0.25 nm for each point in the set of boundary points. The Resnich algorithm is then applied to obtain the spline function and the integral of Eq. 6 is evaluated. If its value is greater than 0.15, δy is incremented by 0.01 nm and the spline is recalculated. This process is repeated until the integral is less than 0.15. When this condition is satisfied, we consider the spline curve to be sufficiently smooth and devoid of oscillations. The differentiability of the spline curve allows us to compute the contact angle $\theta_i = \theta(R_i)$ at the point where the three interfaces meet. The data, along with the extrapolation to infinite radius, is shown in Fig. 4.

The line tension is plotted against the solid/liquid interaction strength in Fig. 5. Its magnitude ($\sim 10^{-10}$ J/m) is consistent with what is known about line tension [11]. The data suggests that the line tension increases with the interaction strength; this trend agrees with the data reported by Werder [6] on similar systems. In all cases we observe

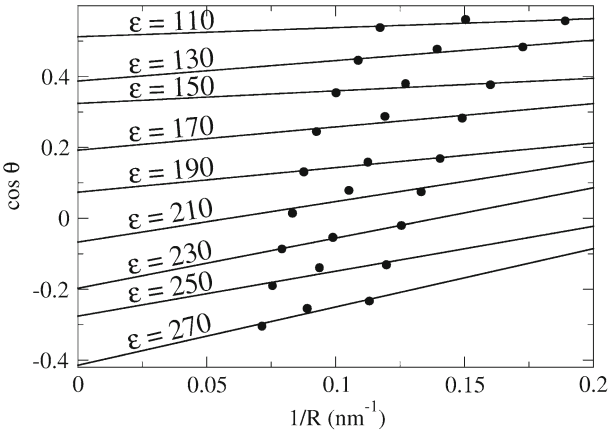

Fig. 4 Calculation of the macroscopic contact angle for a droplet of liquid on a flat solid surface. The microscopic contact angle is plotted against the inverse radius of the three-phase contact line for droplets consisting of 11, 000, 22, 000, and 44, 000 particles. Linear extrapolation to infinite radius yields the macroscopic contact angle, with the slope being the line tension divided by the liquid/vapor surface tension

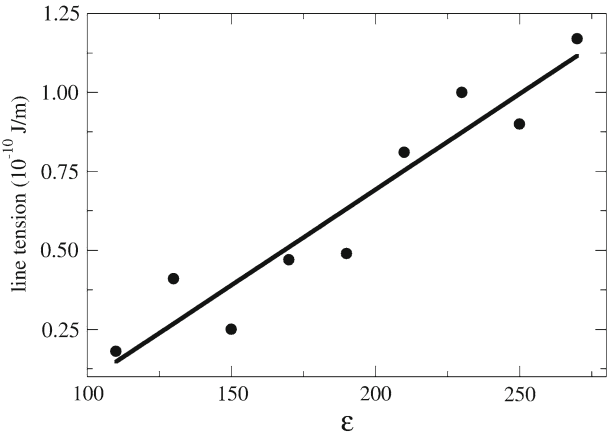

Fig. 5 The three-phase solid/liquid/vapor line tension is plotted as a function of ϵ, along with the best linear fit to the data

a positive line tension, which means that at small radius, the droplet base contracts, increasing the contact angle compared to the macroscopic limit.

Finally, we are ready to compute the solid/liquid surface tension from $\cos\theta_\infty$ using Eq. 1. Two additional quantities are required, namely the liquid/vapor and solid/vapor surface tensions. We use $\gamma_{\rm lv}$ as reported by Shinoda [8]. To estimate $\gamma_{\rm sv}$ we perform the following calculation: the vapor particles are identified by using the liquid/vapor boundary curve from above. The solid/vapor tension is then calculated using the pressure tensor methods discussed below with area $\mathcal{A} = L_x L_y - \pi R_i^2$ (where the quantity subtracted is the space occupied by the droplet). We find that $\gamma_{\rm sv} \approx 0$ for all cases, simply because there are very few vapor particles near the surface, in spite of suggestions to the contrary [12]. The solid/liquid surface tension data is plotted in Fig. 6.

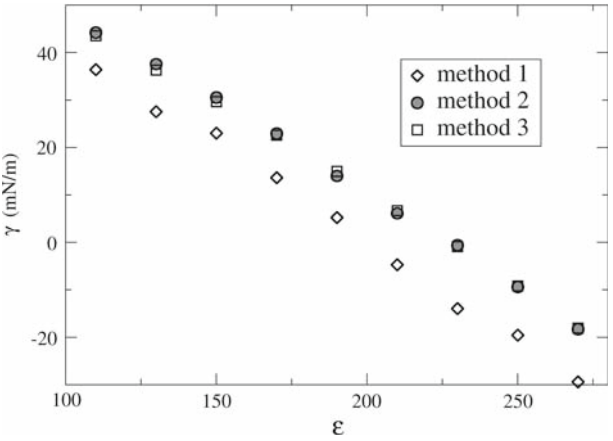

Fig. 6 The surface tension of a flat solid/liquid interface, as a function of ϵ, is plotted for the three methods under consideration: method 1, the contact angle route; method 2, the pressure tensor route, and method 3, the solvation free energy route. A solid surface is classified as hydrophobic if $\gamma > 0$ and as hydrophilic if $\gamma < 0$

3 Method 2: pressure tensor

Continuing with the known routes to calculate the surface tension, we turn our attention to a flat interface as depicted in Fig. 7. The liquid/liquid and solid/liquid interactions are as described above, and we take the solid/vapor interaction to be purely repulsive.

An expression for the surface tension can be derived by using the virial [13,14]. The pressure tensor (or stress tensor) can be defined from the virial as [13–15]

$$P_{ab} = \frac{1}{V}\left(\sum_i p_{ia}p_{ib}/m_i + \sum_i r_{ia}f_{ib}\right), \tag{8}$$

where ab is a component of the pressure tensor, i is the particle index, p is the momentum of particle i, m its mass, r its position, and f is the force. The pressure tensor is thus

$$P = \begin{pmatrix} P_{xx} & P_{xy} & P_{xz} \\ P_{yx} & P_{yy} & P_{yz} \\ P_{zx} & P_{zy} & P_{zz} \end{pmatrix}. \tag{9}$$

In our system, the off-diagonal components average to zero and the diagonal components have normal ($P_n = P_{zz}$) and tangential $P_t(z) = \frac{1}{2}(P_{xx} + P_{yy})$ contributions relative to the interfaces (Fig. 7).

The surface tension can be defined by the well-known expression [16]

$$\gamma = \int_{-\infty}^{\infty} dz[P_n - P_t(z)]. \tag{10}$$

The tangential pressure is different from the normal pressure only in the vicinity of the interfaces. There is a contribution from each interface. Our simulations are performed

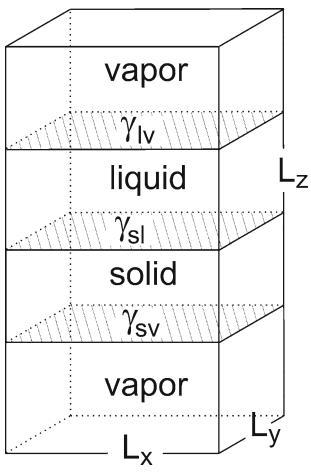

Fig. 7 The simulation unit cell is shown for the pressure tensor route to calculate surface tension. The unit cell is replicated in all three dimensions to set up periodic boundary conditions

in an orthorhombic box as depicted in Fig. 7 with sides L_x, L_y, L_z, where the area of the interface is $\mathcal{A} = L_x L_y$. The total surface tension can be rewritten as

$$\gamma = L_z(P_n - \bar{P}_t), \tag{11}$$

where $\bar{P}_t$ is the average tangential pressure $P_t(z)$. Note that the box size dependence of Eq. 11 is $1/\mathcal{A}$ since $V = L_x L_y L_z$.

We can divide the total surface tension into contributions from the individual surface tensions as [17]

$$\gamma = \gamma_{\mathrm{sl}} + \gamma_{\mathrm{lv}} + \gamma_{\mathrm{sv}}. \tag{12}$$

This is possible because the interfaces are separated from each other and do not interact—i.e., there is a bulk phase region between each interface. From previous work, we have $\gamma_{\mathrm{lv}} = 71\,\mathrm{mN/m}$ [8]. Also, $\gamma_{\mathrm{sv}} \approx 0$, because the surface is constructed to be purely repulsive on the vapor side.

Thus we can determine γ_{sl} as

$$\gamma_{\mathrm{sl}} = \langle P_n - P_t \rangle - \gamma_{\mathrm{lv}}. \tag{13}$$

The resulting solid/liquid surface tension data is plotted in Fig. 6.

4 Method 3: solvation free energy

In this section we introduce a new method to calculate solid/liquid surface tension, based on the thermodynamic definition of surface tension, γ, given by [18]

$$\gamma \equiv \left(\frac{\partial G}{\partial \mathcal{A}}\right)_{N,P,T}, \tag{14}$$

where G is the Gibbs free energy and $\mathcal{A}$ is the interfacial area.

Motivated by this definition, we will compute the solvation free energy of a spherical solid of radius R and recover the flat result by taking the limit as $R \to \infty$. In order to do this, we must adapt the flat potential $U_{\mathrm{sl}}(d) = a\epsilon\sigma^9 d^{-6} - b\epsilon\sigma^6 d^{-3}$ to a curved solid geometry. This is straightforward, and is done as follows [19].

Suppose that an individual atomic crystal lattice site in the solid interacts with a particle in the liquid via a distance-dependent potential energy $u(r)$. Approximating the solid as a continuum with number density $\rho = N/V$ that occupies the semi-infinite region $z \leq 0$, a liquid particle at height $z > 0$ interacts with the entire solid object as

$$\begin{aligned} U(z) &= \int_z^\infty dr \int_0^{2\pi} d\theta \int_{\pi - \cos^{-1}(z/r)}^{\pi} d\phi\, r^2 \sin\phi\, \rho u(r) \\ &= 2\pi\rho \int_z^\infty r u(r)[r - z]dr. \end{aligned} \tag{15}$$

Two derivatives yield

$$u(\xi) = \frac{U''(\xi)}{2\pi\rho\xi}. \tag{16}$$

Using expressions (16) and $U_{\mathrm{sl}}(d) = a\epsilon\sigma^9 d^{-6} - b\epsilon\sigma^6 d^{-3}$, we obtain

$$u_{\mathrm{sl}}(r) = \frac{21a\epsilon\sigma^9}{\pi\rho} r^{-9} - \frac{6b\epsilon\sigma^6}{\pi\rho} r^{-6} \tag{17}$$

as the potential energy between a particle in the liquid and a particle in the solid. Now, we once again approximate the solid as a continuum with number density $\rho = N/V$, but this time as a sphere of radius R. A liquid particle interacts with the entire solid sphere as

$$\begin{aligned} U(d, R) &= \int_0^R dr \int_0^{2\pi} d\theta \int_0^{\pi} d\phi \rho r^2 \sin\phi u([r^2 + (d+R)^2 - 2r\cos\phi(d+R)]^{1/2}) \\ &= \frac{4a\epsilon\sigma^9 R^3}{5d^6} \frac{35d^4 + 140Rd^3 + 252R^2d^2 + 224R^3d + 80R^4}{(d+R)(d+2R)^6} \\ &\quad - \frac{8b\epsilon\sigma^6 R^3}{d^3(d+2R)^3}, \end{aligned} \tag{18}$$

where d is the distance between the liquid particle and the solid.

We now change variables from $U(d, R)$ to $U(r, R)$ where $r = d + R$, the distance between the centers of mass of the solid sphere and the liquid particle. Let us now consider the significance of the two partial derivatives $\partial U/\partial r$ and $\partial U/\partial R$. First, $-\partial U/\partial r$ (the gradient of the potential) gives the force that acts between the two particles on their respective centers of mass. This is the force used to move the particles during a molecular dynamics simulation. Second, $\sum_i -\partial U/\partial R$, summed over all liquid particles i, represents the force acting on the sphere radius. However, the sphere radius is fixed and hence does not experience this force. Conceptually, to balance this force so that the sphere radius experiences a net force of zero, we should apply an external force to the sphere radius of $\sum_i \partial U/\partial R$ at each step of the simulation. However, we do not actually apply this external force since the sphere radius is in no danger of changing. Nonetheless, we may calculate the required external restoring force on the sphere radius, known as the force of constraint, and record its value during a computer simulation. Its average value over an equilibrium simulation is called the mean force of constraint; let us denote it by PMF(R). By performing separation simulations with spheres of different radii, we can integrate PMF(R) starting from $R = 0$ to obtain the solvation free energy $G(R)$. $G(R)$ can be thought of as the free energy cost of "growing" the sphere into water. It can also be thought of as the free energy cost of transferring a spherical solid of radius R from an ideal gas reference state to a liquid. We have verified the validity of the PMF route to $G(R)$ by performing free energy calculations corresponding to the later interpretation, where a radius R sphere is pulled

from the vapor phase, through the liquid/vapor interface, and into the liquid phase in a simulation system of an infinitely extended, thick, slab of liquid.

From the definition of surface tension in Eq. 14, we have

$$\lim_{R\to\infty} \frac{G(R)}{4\pi R^2} = \gamma. \tag{19}$$

This is because the short range nature of the potential energy functions means that, for large R, $G(R)$ becomes interface-dominated. We performed 30 equilibrium MD simulations of 10 ns each for spheres of radius $R = 0.1,\ 0.2,\ 0.3,\ \ldots,\ 3.0$ nm embedded in a large box of water. The data in the range $R \in [1.0\,\text{nm},\ 3.0\,\text{nm}]$ is fit to the three-parameter function $G(R)/4\pi R^2 = \gamma + aR^{-b}$. The fits are shown in Fig. 8 along with the data points; we feel the quality of the fit justifies our choice. Huang [20] used a power series expansion in $1/R$ truncated at first order. The γ values are shown in Fig. 6. The exponents b are monotone increasing with ϵ, and range from 0.95 to 1.28 for the range of ϵ studied.

Rather than performing simulations of small radius spheres and extrapolating the data to infinite radius, let us consider the possibility of extending the method, formally, to infinite radius. In other words, let us consider performing a simulation of a flat solid/liquid interface, and ask whether the current method gives us access to the surface tension or not. Clearly it is not possible to calculate $G(R)$, because this would require us to integrate the PMF from $R = 0$ to ∞. However, we can directly calculate the surface tension from the PMF by

$$\gamma = \lim_{R\to\infty} \frac{\text{PMF}(R)}{8\pi R} \tag{20}$$

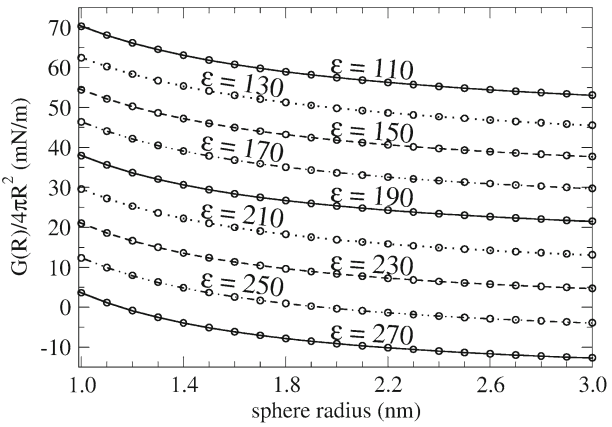

Fig. 8 For each value of ϵ, the solvation free energy $G(R)$ of a solid sphere of radius $R = 0.1,\ 0.2,\ 0.3,\ \ldots,\ 3.0$ nm is calculated from MD simulations according to method 3. The solvation free energy per unit area is fit to the three-parameter function $G(R)/4\pi R^2 = \gamma + aR^{-b}$ over the range $R \in [1.0\,\text{nm},\ 3.0\,\text{nm}]$. The fits are shown along with the data points. The exponents b are monotone increasing with ϵ and lie in the range $b \in [0.95,\ 1.28]$

for the following reason: writing $G(R)/4\pi R^2 = \gamma + h(R)$, where $h(R) \to 0$ as $R \to \infty$, we have $\mathrm{PMF}(R)/8\pi R = \gamma + h(R) + Rh'(R)/2$ since PMF is the derivative of $G(R)$. Equation 20 is valid if $Rh'(R)/2 \to 0$ as $R \to \infty$, which holds since we estimated numerically that $h(R) = aR^{-b}$ with $b \in (0.95,\ 1.28)$.

The limiting expressions for the potential energy and its derivatives are also well-defined: for example it is straightforward to verify that Eq. 18 reduces to $U_{\mathrm{sl}}(d) = a\epsilon\sigma^9 d^{-6} - b\epsilon\sigma^6 d^{-3}$, $\lim_{R\to\infty} U(d, R) = U_{\mathrm{sl}}(d)$. Unfortunately, there are two problems blocking the use of the sphere method for flat interfaces. The first problem is the scaling of $\mathrm{PMF}(R)$ with R, and the second problem arises from the use of periodic boundary conditions in computer simulations. We will now discuss these problems in detail.

Only a patch of the flat solid/liquid interface can be simulated, of area $\mathcal{A} = L \times L$ as shown in Fig. 9a. Periodic boundary conditions in the directions parallel to the interface mimic an infinite solid/liquid interface, but the liquid atoms contribute to the PMF only in the $L \times L$ patch shown. Deforming this patch onto the surface of a sphere of radius R gives the patch shown in Fig. 9b, of area $\mathcal{A} = 2RL\sin(L/2R)$, which approaches L^2 as $R \to \infty$. Analogous to the flat case, we should only use the liquid atoms above the curved patch to compute the PMF corresponding to this patch. To recover the full PMF, a sum over patches must be performed. With L fixed and R increasing, the number of patches we need grows like R^2. The full PMF, however, grows like $8\pi R\gamma$ for large R. We conclude that in the limit $R \to \infty$, the contribution to the PMF from a single patch goes to zero. Hence the sphere method does not allow us to compute γ for the flat geometry. Second, the sphere method, for finite R, does not use periodic boundary conditions to replicate the patches. Rather, each patch is explicitly simulated because the entire sphere fits inside the simulation box. For reasons of mechanical equilibrium, this implies that the components of the pressure tensor normal and tangential to the interface are related by a differential equation [13]. In contrast, a planar interface has independent normal and tangential pressure tensor

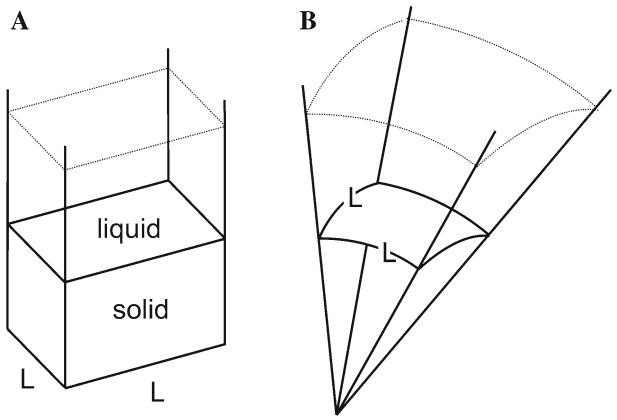

Fig. 9 A flat solid/liquid interface of area L^2 is shown in panel A. Thought of as a patch of a sphere of infinite radius, panel B shows the corresponding patch for a finite sphere, with surface area $2RL\sin(L/2R)$

values, which is why they both appear explicitly in Eq. 11; the sphere method lacks any explicit contributions from tangential forces.

5 Conclusions

We have presented three topologically different methods for computing the surface tension between a liquid and a flat solid. In method 1, a hemispherical droplet of liquid surrounded by vapor rests on a flat solid surface. The surface tension is obtained by measuring the angle at which the liquid/vapor boundary meets the solid surface. The line tension associated with the three-phase boundary is calculated and is shown to be proportional to the strength of the solid/liquid interaction. In method 2, all three phases are also present, but only meet in pairs at planar interfaces. The pressure tensor is used to compute the surface tension. In method 3, a spherical solid is surrounded by liquid, and the vapor phase is absent. The solvation free energy of the solid, which is used to obtain the surface tension, is calculated by a novel method based on constrained molecular dynamics. Although method 2 is the most efficient because no extrapolation is required, it also gives the least amount of information. Method 1 allows the line tension to be computed, which is crucial to understanding the behavior of nanoscale systems with three-phase boundaries. Method 3 gives access to spherical solids, opening the door to colloid science. Methods 2 and 3 are in perfect agreement, whereas method 1 systematically underestimates the surface tension as a function of the hydrophobicity/hydrophilicity of the surface (see Fig. 6). We do not understand why this discrepancy exists. We will continue to work on this problem.

Acknowledgements The authors acknowledge the Donors of the American Chemical Society Petroleum Research Fund for partial support of this research. Dr. Moore would like to acknowledge that this research was supported in part by a gift from the H.O. West Foundation, a grant from the University of the Sciences in Philadelphia (USP), a grant from the National Institute of Health (1R15GM075990-01), and grants from the National Science Foundation (CHE-0420556 and CCF-0622162). The authors would also like to acknowledge the Texas Advanced Computing Center (TACC) at The University of Texas at Austin for providing HPC resources that have contributed to the research results reported within this paper.

References

1. Y. Lin, H. Skaff, T. Emrick, A.D. Dinsmore, T.P. Russell, Science **299**, 226–229 (2003)
2. D. Wang, H. Duan, H. Möhwald, Soft Matter **1**, 412–416 (2005)
3. B.P. Binks, J.H. Clint, Languir **18**, 1270–1273 (2002)
4. E. Salomons, M. Mareschal, J. Phys. Condens. Matter **3**, 3645–3661 (1991)
5. J.Y. Wang, S. Betelu, B.M. Law, Phys. Rev. E **63**, 031601 (2001)
6. T. Werder, J.H. Walther, R.L. Jaffe, T. Halicioglu, P. Koumoutsakos, J. Phys. Chem. B **107**, 1345–1352 (2003)
7. N. Giovambattista, P.G. Debenedetti, P.J. Rossky, J. Phys. Chem. B **111**, 9581–9587 (2007)
8. W. Shinoda, R. Devane, M.L. Klein, Mol. Simul. **33**, 27–36 (2007)
9. S.O. Nielsen, G. Srinivas, M.L. Klein, J. Chem. Phys. **123**, 124907 (2005)
10. C.H. Reinsch, Numer. Math. **10**, 177–183 (1967); **16**, 451–454 (1971)
11. J. Drelich, Colloids Surf. A **116**, 43–54 (1996)
12. S.M. Dammer, D. Lohse, Phys. Rev. Lett. **96**, 206101 (2006)
13. M.P. Allen, D.J. Tildesley, *Computer Simulations of Liquids* (Oxford University Press, Oxford, 1987)
14. J.H. Irving, J.G. Kirkwood, J. Chem. Phys. **18**, 817–829 (1950)

15. Y. Zhang, S.E. Feller, B.R. Brooks, R.W. Pastor, J. Chem. Phys. **103**, 10252–10266 (1995)
16. T.L. Hill, *Statistical Thermodynamics* (Addison-Wesley, Reading, MA 1962)
17. S.E. Feller, Y. Zhang, R.W. Pastor, J. Chem. Phys. **103**, 10267–10276 (1995)
18. W.J. Moore, *Physical Chemistry*, 4th edn. (Prentice-Hall, New Jersey, 1972)
19. S.O. Nielsen, G. Srinivas, C.F. Lopez, M.L. Klein, Phys. Rev. Lett. **94**, 228301 (2005)
20. D.M. Huang, P.L. Geissler, D. Chandler, J. Phys. Chem. B **105**, 6704–6709 (2001)